ISSN 0965-5425, Computational Mathematics and Mathematical Physics, 2016, Vol. 56, No. 6, pp. 1128–1141. © Pleiades Publishing, Ltd., 2016.
Original Russian Text © D.I. Petrov, I.B. Petrov, A.V. Favorskaya, N.I. Khokhlov, 2016, published in Zhurnal Vychislitel'noi Matematiki i Matematicheskoi Fiziki, 2016, Vol. 56, No. 6, pp. 1149–1163.

Dedicated to the memory of O.M. Belotserkovskii

Numerical Solution of Seismic Exploration Problems in the Arctic Region by Applying the Grid-Characteristic Method

D. I. Petrov, I. B. Petrov, A. V. Favorskaya, and N. I. Khokhlov

Moscow Institute of Physics and Technology (State University), Institutskii per. 9, Dolgoprudnyi, Moscow oblast, 141700 Russia

e-mail: petrov@mipt.ru

Received November 9, 2015

Abstract—The goal of this paper is the numerical solution of direct problems concerning hydrocarbon seismic exploration on the Arctic shelf. The task is addressed by solving a complete system of linear elasticity equations and a system of acoustic field equations. Both systems are solved by applying the grid-characteristic method, which takes into account all wave processes in a detailed and physically correct manner and produces a solution near the boundaries and interfaces of the integration domain, including the interface between the acoustic and linear elastic media involved. The seismograms and wave patterns obtained by numerically solving these systems are compared. The effect of ice structures on the resulting wave patterns is examined.

Keywords: grid-characteristic method, numerical simulation, seismic exploration on Arctic shelf, icebergs, acoustic media, linear elastic media.

DOI: 10.1134/S0965542516060208

INTRODUCTION

According to the estimates presented in [1], the hydrocarbon resources in the Arctic region amount to 25% of the world's reserves. Seismic exploration in this region has been conducted for more than 30 years (see [2]). Seismic surveys on the Arctic shelf are complicated by the presence of water and ice layers [3] and ice structures (icebergs, pressure ridges), which not only hamper the collection of data, but also affect the resulting seismograms. Physical experiments aimed at evaluating these effects are expensive and fail to provide a complete wave pattern for the objects under study. Additionally, all characteristics are measured with errors and the collection of data in the Arctic region is complicated by heavy operating conditions [4–6]. At the same time, numerical simulation makes it possible to investigate all spatial dynamical wave processes and determine the contributions of waves of various types to recorded seismograms.

The numerical solution of seismic exploration problems is based primarily on ray methods [7]. In [8–13] such problems were solved using finite element and spectral element methods, including high-order accurate ones. Finite-difference schemes adapted to the simulation of seismic problems were presented in [11, 13, 14].

By applying the grid-characteristic method [15–22] with suitable conditions specified on the boundaries and interfaces of the integration domain [15], the above problems can be studied by performing series of numerical experiments. In this paper, we compare wave patterns and seismograms obtained in the numerical simulation of geological rocks by applying the linear elasticity system and the acoustic field system. Additionally, the effect of icebergs on wave processes in seismic exploration is analyzed.

FORMULATION OF THE PROBLEM

Following [23], the state of a linear elastic continuum is governed by the equations

$$\rho \partial_t \mathbf{v} = (\nabla \cdot \boldsymbol{\sigma})^{\mathrm{T}}, \tag{1}$$

$$\partial_t \boldsymbol{\sigma} = \lambda(\nabla \cdot \mathbf{v})\mathbf{I} + \mu(\nabla \otimes \mathbf{v} + (\nabla \otimes \mathbf{v})^{\mathrm{T}}). \tag{2}$$

Equation (1) is a local equation of motion. Here, ρ is the material density, $\mathbf{v}$ is the velocity, and $\boldsymbol{\sigma}$ is the Cauchy stress tensor. In (2), λ and μ are the Lamé constants, which determine the properties of the elastic material.

In (1), (2), and below, we use the following mathematical notation:

$\partial_t a \equiv \dfrac{\partial a}{\partial t}$ is the partial derivative of a field a with respect to t;

$\mathbf{a} \otimes \mathbf{b}$ is the tensor product of vectors $\mathbf{a}$ and $\mathbf{b}$, $(\mathbf{a} \otimes \mathbf{b})^{ij} = a^i b^j$; and

$\mathbf{I}$ is the second-rank unit tensor.

Consider a system of equations describing an acoustic field, including liquids, in the approximation of an ideal incompressible fluid [24]. Specifically, the pressure p and the velocity $\mathbf{v}$ are governed by the equations

$$\rho \mathbf{v}_t = -\nabla p, \tag{3}$$

$$p_t = -c^2 \rho(\nabla \cdot \mathbf{v}). \tag{4}$$

In Eq. (4), c denotes the speed of sound in the acoustic medium.

GRID-CHARACTERISTIC METHOD

In the two-dimensional case, systems (1), (2) and (3), (4) can be represented in the form

$$\mathbf{q}_t + \mathbf{A}_1^{2\mathrm{D}} \mathbf{q}_x + \mathbf{A}_2^{2\mathrm{D}} \mathbf{q}_y = 0, \tag{5}$$

while, in the three-dimensional case, they can be rewritten as

$$\mathbf{q}_t + \mathbf{A}_1^{3\mathrm{D}} \mathbf{q}_x + \mathbf{A}_2^{3\mathrm{D}} \mathbf{q}_y + \mathbf{A}_3^{3\mathrm{D}} \mathbf{q}_z = 0. \tag{6}$$

Next, splitting in two or three directions is performed and, for each direction, we obtain a system of the form

$$\mathbf{q}_t + \mathbf{A}_1 \mathbf{q}_x = 0 \tag{7}$$

with exact expressions

$$\mathbf{q}(x, y, t + \tau) = \sum_{j=1}^{J} \mathbf{X}_j^{2\mathrm{D},1} \bar{q}(x - c_j^{2\mathrm{D},1}\tau, y, t), \tag{8}$$

$$\mathbf{q}(x, y, z, t + \tau) = \sum_{j=1}^{J} \mathbf{X}_j^{3\mathrm{D},1} \mathbf{q}(x - c_j^{3\mathrm{D},1}\tau, y, z, t) \tag{9}$$

in the two- and three-dimensional cases, respectively. In (7) and below, $\mathbf{A}_1$ denotes the matrices $\mathbf{A}_1^{2\mathrm{D}}$ and $\mathbf{A}_1^{3\mathrm{D}}$ in the two- and three-dimensional case, respectively. In (8) and (9), $\mathbf{X}_j^{2\mathrm{D},1}$ are matrices that can be expressed in terms of elements of $\mathbf{A}_1^{2\mathrm{D}}$, $c_j^{2\mathrm{D},1}$ are the eigenvalues of $\mathbf{A}_1^{2\mathrm{D}}$, $\mathbf{X}_j^{3\mathrm{D},1}$ are matrices that can be expressed in terms of elements of $\mathbf{A}_1^{3\mathrm{D}}$, $c_j^{3\mathrm{D},1}$ are the eigenvalues of $\mathbf{A}_1^{3\mathrm{D}}$, τ is the time step, and J is the number of eigenvalues of the matrix $\mathbf{A}_1$. Suppose that $\mathbf{A}_1$ has a set J^+ of positive eigenvalues, a set J^- of negative eigenvalues, and a set J^0 of zero eigenvalues.

The matrices $\mathbf{X}_j^1$ (both $\mathbf{X}_j^{2\mathrm{D},1}$ and $\mathbf{X}_j^{3\mathrm{D},1}$) satisfy the relation

$$\sum_{j=1}^{J} \mathbf{X}_j^1 = \mathbf{I}. \tag{10}$$

Accordingly, the matrices $\mathbf{X}_j^1$ corresponding to zero eigenvalues can be expressed as

$$\sum_{j\in J^0}\mathbf{X}_j^1 = \mathbf{I} - \sum_{j\in J^{0+}}\mathbf{X}_j^1 - \sum_{j\in J^-}\mathbf{X}_j^1. \tag{11}$$

Taking into account (8) and (9), we obtain their equivalents

$$\mathbf{q}(x,y,t+\tau) = \mathbf{q}(x,y,t) + \sum_{j\in J^+\cup J^-}\mathbf{X}_j^{2\mathrm{D},1}(\mathbf{q}(x-c_j^{2\mathrm{D},1}\tau,y,t) - \mathbf{q}(x,y,t)), \tag{12}$$

$$\mathbf{q}(x,y,z,t+\tau) = \mathbf{q}(x,y,z,t) + \sum_{j\in J^+\cup J^-}\mathbf{X}_j^{3\mathrm{D},1}(\mathbf{q}(x-c_j^{2\mathrm{D},1}\tau,y,z,t) - \mathbf{q}(x,y,z,t)). \tag{13}$$

The matrix $\mathbf{A}_1$ has a set of eigenvectors, so it can be represented in the form

$$\mathbf{A}^1 = (\mathbf{\Omega}^1)^{-1}\mathbf{\Lambda}^1\mathbf{\Omega}^1. \tag{14}$$

Here, $(\mathbf{\Omega}^1)^{-1}$ is the matrix composed of the eigenvectors of $\mathbf{A}_1$, while $\mathbf{\Lambda}^1$ is a diagonal matrix with elements being the eigenvalues of $\mathbf{A}_1$.

The computations based on formulas (12) and (13) are divided into three stages. At the first stage, all vectors $\mathbf{q}(x,y,t)$ or $\mathbf{q}(x,y,z,t)$ are multiplied by the matrix $\mathbf{\Omega}^1$:

$$\boldsymbol{\omega}(x,y,t) = \mathbf{\Omega}^1\mathbf{q}(x,y,t), \tag{15}$$

$$\boldsymbol{\omega}(x,y,z,t) = \mathbf{\Omega}^1\mathbf{q}(x,y,z,t). \tag{16}$$

At the second stage, the following expressions are found in the two- and three-dimensional cases, respectively:

$$\boldsymbol{\omega}(x,y,t+\tau) = \boldsymbol{\omega}(x,y,t) + \sum_{j\in J^+\cup J^-}\boldsymbol{\omega}(x-c_j^{2\mathrm{D},1}\tau,y,t) - \boldsymbol{\omega}(x,y,t), \tag{17}$$

$$\boldsymbol{\omega}(x,y,z,t+\tau) = \boldsymbol{\omega}(x,y,z,t) + \sum_{j\in J^+\cup J^-}\boldsymbol{\omega}(x-c_j^{3\mathrm{D},1}\tau,y,z,t) - \boldsymbol{\omega}(x,y,z,t). \tag{18}$$

At the third stage, back substitutions of coordinates yield

$$\mathbf{q}(x,y,z,t) = (\mathbf{\Omega}^1)^{-1}\boldsymbol{\omega}(x,y,z,t), \tag{19}$$

$$\mathbf{q}(x,y,z,t+\tau) = (\mathbf{\Omega}^1)^{-1}\boldsymbol{\omega}(x,y,z,t+\tau). \tag{20}$$

The use of formulas (17) and (18) is equivalent to solving the independent advection equations

$$(\omega_j)_t + c_j^1(\omega_j)_x = 0. \tag{21}$$

Here and below, c_j^1 denotes the eigenvalues $c_j^{2\mathrm{D},1}$ and $c_j^{3\mathrm{D},1}$ in the two- and three-dimensional cases, respectively. Then Eqs. (21) are solved as described in [17] and, next, the same procedure is performed in the y direction or the y and z directions in order to solve systems similar to (7).

BOUNDARY AND CONTACT CORRECTORS

Relying on the family of grid-characteristic methods, we can design numerical algorithms that perform well near the boundaries and interfaces of the integration domain and preserve the order of accuracy of the method used to compute the solution at interior nodes of the integration domain.

Suppose that the boundary condition is written in matrix form as

$$\mathbf{D}\mathbf{q}(x_\mathrm{b},y_\mathrm{b},t+\tau) = \mathbf{d}, \tag{22}$$

$$\mathbf{D}\mathbf{q}(x_\mathrm{b},y_\mathrm{b},z_\mathrm{b},t+\tau) = \mathbf{d} \tag{23}$$

in the two- and three-dimensional cases, respectively, where $\mathbf{q}(x_\mathrm{b},y_\mathrm{b},t+\tau)$ and $\mathbf{q}(x_\mathrm{b},y_\mathrm{b},z_\mathrm{b},t+\tau)$ are the velocity and stress tensor components for system (1), (2) or the velocity and pressure for system (3), (4) at a boundary point at the next integration step.

For each direction, there are two types of correctors (for the left and right boundaries); i.e., overall there are six and four types of boundary correctors in the three- and two-dimensional cases, respectively. To be definite, we consider one of them. Suppose that the characteristics corresponding to the negative eigenvalues of $\mathbf{A}_1$ go beyond the integration domain in the x direction.

Then, according to (15)–(20), at the stage of finding the solution at interior nodes, we calculate

$$\mathbf{q}(x_\mathrm{b}, y_\mathrm{b}, t+\tau) = \mathbf{q}(x_\mathrm{b}, y_\mathrm{b}, t) + \sum_{j\in J^+} \mathbf{X}_j^{2\mathrm{D},\mathrm{l}}(\mathbf{q}(x_\mathrm{b} - c_j^{2\mathrm{D},\mathrm{l}}\tau, y_\mathrm{b}, t) - \mathbf{q}(x_\mathrm{b}, y_\mathrm{b}, t)), \tag{24}$$

$$\mathbf{q}(x_\mathrm{b}, y_b, z_\mathrm{b}, t+\tau) = \mathbf{q}(x_\mathrm{b}, y_\mathrm{b}, z_\mathrm{b}, t) + \sum_{j\in J^+} \mathbf{X}_j^{3\mathrm{D},\mathrm{l}}(\mathbf{q}(x_\mathrm{b} - c_j^{2\mathrm{D},\mathrm{l}}\tau, y_\mathrm{b}, z_\mathrm{b}, t) - \mathbf{q}(x_\mathrm{b}, y_\mathrm{b}, z_\mathrm{b}, t)). \tag{25}$$

The matrix $\mathbf{\Omega}^{*,\mathrm{out}}$ consists of the eigenvectors corresponding to the negative eigenvalues.

At a boundary point, the corrector is given by the formulas

$$\mathbf{q}(x_\mathrm{b}, y_\mathrm{b}, t+\tau) = \mathbf{F}\mathbf{q}^{\mathrm{in}}(x_\mathrm{b}, y_\mathrm{b}, t+\tau) + \mathbf{\Phi}\mathbf{d}, \tag{26}$$

$$\mathbf{q}(x_\mathrm{b}, y_\mathrm{b}, z_\mathrm{b}, t+\tau) = \mathbf{F}\mathbf{q}^{\mathrm{in}}(x_\mathrm{b}, y_\mathrm{b}, z_\mathrm{b}, t+\tau) + \mathbf{\Phi}\mathbf{d} \tag{27}$$

in the two- and three-dimensional cases, respectively. Moreover, conditions (22) and (23) are satisfied with the same order of convergence as that of the method used to solve system (1), (2) and, accordingly, to find (24) and (25).

In (27), the matrices $\mathbf{\Phi}$ and $\mathbf{F}$ are calculated using the formulas

$$\mathbf{\Phi} = \mathbf{\Omega}^{*,\mathrm{out}}(\mathbf{D}\mathbf{\Omega}^{*,\mathrm{out}})^{-1}, \tag{28}$$

$$\mathbf{F} = \mathbf{I} - \mathbf{\Phi}\mathbf{D}, \tag{29}$$

and, in (28), the matrix $(\mathbf{D}\mathbf{\Omega}^{*,\mathrm{out}})^{-1}$ is found so that

$$(\mathbf{D}\mathbf{\Omega}^{*,\mathrm{out}})^{-1}\mathbf{D}\mathbf{\Omega}^{*,\mathrm{out}} = \mathbf{I}. \tag{30}$$

For system (1), (2), boundary conditions can be specified as a given boundary velocity, a given external force density, mixed and nonreflecting conditions, and no-slip, free slip, or dynamic friction at contacts [25]. For system (3), (4), boundary conditions can be specified in the form of a given normal boundary velocity, a given pressure, or a contact condition. A contact condition is also set at the interface between the linear elastic and acoustic media [16].

Suppose system (1), (2) is solved in the subdomain a of the integration domain, while system (3), (4) is solved in the subdomain b of the integration domain, and let $\mathbf{p}$ be the outward normal vector to the body a. Consider the contact condition between them in the three-dimensional case. Then system (1), (2) has three outgoing characteristics, while system (3), (4) has one outgoing characteristic. Thus, to find all four outgoing characteristics, we need the contact conditions

$$p^{b,n+1} = -(\mathbf{\sigma}^{a,n+1}\cdot\mathbf{p})\cdot\mathbf{p}, \tag{31}$$

$$\mathbf{\sigma}^{a,n+1}\cdot\mathbf{p} - (\mathbf{\sigma}^{a,n+1}\cdot\mathbf{p})\cdot\mathbf{p} = 0, \tag{32}$$

$$\mathbf{v}^{a,n+1}\cdot\mathbf{p} = \mathbf{v}^{b,n+1}\cdot\mathbf{p}. \tag{33}$$

Condition (31) means that the normal surface force density exerted by the solid is equal to the pressure in the ideal fluid, condition (32) ensures that the tangential surface force density exerted by the solid is zero, and (33) states that the normal velocities in the fluid and the solid are equal to each other.

LINEAR ELASTIC MEDIA

To be definite, let the vector $\mathbf{n}$ be directed along the x axis and the vectors $\mathbf{n}_1$ and $\mathbf{n}_2$ (or only $\mathbf{n}_1$ in the two-dimensional case) form, together with $\mathbf{n}$, a Cartesian coordinate system. Define the symmetric second-rank tensors

$$\mathbf{N}_{ij} = \frac{1}{2}(n_i \otimes n_j + n_j \otimes n_i), \tag{34}$$

where the indices vary from 0 to 2 and $\mathbf{n}_0$ means the vector $\mathbf{n}$.

The action of the matrix $\mathbf{A}_1$ on the vector of unknowns defined as

$$\mathbf{q} = \begin{bmatrix} \mathbf{v} \\ \boldsymbol{\sigma} \end{bmatrix} = \begin{bmatrix} v_1 & v_2 & v_3 & \sigma_{11} & \sigma_{22} & \sigma_{33} & \sigma_{23} & \sigma_{13} & \sigma_{12} \end{bmatrix}^{\mathrm{T}} \tag{35}$$

in the three-dimensional case and as

$$\mathbf{q} = \begin{bmatrix} \mathbf{v} \\ \boldsymbol{\sigma} \end{bmatrix} = \begin{bmatrix} v_1 & v_2 & \sigma_{11} & \sigma_{22} & \sigma_{12} \end{bmatrix}^{\mathrm{T}} \tag{36}$$

in the two-dimensional case can be written as

$$\mathbf{A}_1 \begin{bmatrix} \mathbf{v} \\ \boldsymbol{\sigma} \end{bmatrix} = -\begin{bmatrix} \dfrac{1}{\rho}(\boldsymbol{\sigma} \cdot \mathbf{n}) \\ \lambda(\mathbf{n} \cdot \mathbf{v})\mathbf{I} + \mu(\mathbf{n} \otimes \mathbf{v} + \mathbf{v} \otimes \mathbf{n}) \end{bmatrix}. \tag{37}$$

The matrices $\mathbf{A}_1^{3\mathrm{D}}$, $\mathbf{A}_2^{3\mathrm{D}}$, and $\mathbf{A}_3^{3\mathrm{D}}$ have an identical set of eigenvalues:

$$\{c_p, -c_p, c_s, -c_s, c_s, -c_s, 0, 0, 0\}. \tag{38}$$

The matrices $\mathbf{A}_1^{2\mathrm{D}}$ and $\mathbf{A}_2^{2\mathrm{D}}$ also have the same eigenvalues:

$$\{c_p, -c_p, c_s, -c_s, 0\}. \tag{39}$$

In the two-dimensional case, the action of the matrix $\boldsymbol{\Omega}_1$ from (15) on the unknown vector (36) can be represented as

$$\omega_{1,2} = \left(\boldsymbol{\Omega}_1 \begin{bmatrix} \mathbf{v} \\ \boldsymbol{\sigma} \end{bmatrix}\right)_{1,2} = \mathbf{n} \cdot \mathbf{v} \mp \frac{1}{c_p \rho} \mathbf{N}_{00} \div \boldsymbol{\sigma}, \tag{40}$$

$$\omega_{3,4} = \mathbf{n}_1 \cdot \mathbf{v} \mp \frac{1}{c_s \rho} \mathbf{N}_{01} \div \boldsymbol{\sigma}, \tag{41}$$

$$\omega_5 = \left(\mathbf{N}_{11} - \frac{\lambda}{\lambda + 2\mu} \mathbf{N}_{00}\right) \div \boldsymbol{\sigma}. \tag{42}$$

In the three-dimensional case, the action of the matrix $\boldsymbol{\Omega}_1$ from (16) on the unknown vector (35) can be represented by (40), (41), and the expressions

$$\omega_{5,6} = \mathbf{n}_2 \cdot \mathbf{v} \mp \frac{1}{c_s \rho} \mathbf{N}_{02} \div \boldsymbol{\sigma}, \tag{43}$$

$$\omega_7 = \mathbf{N}_{12} \div \boldsymbol{\sigma}, \tag{44}$$

$$\omega_8 = (\mathbf{N}_{11} - \mathbf{N}_{22}) \div \boldsymbol{\sigma}, \tag{45}$$

$$\omega_9 = \left(\mathbf{N}_{11} + \mathbf{N}_{22} - \frac{2\lambda}{\lambda + 2\mu} \mathbf{N}_{00}\right) \div \boldsymbol{\sigma}. \tag{46}$$

In the two-dimensional case, the action of the matrix $(\boldsymbol{\Omega}_1)^{-1}$ from (19) on the vector $\boldsymbol{\omega}$ can be represented as

$$\begin{bmatrix} \mathbf{v} \\ \boldsymbol{\sigma} \end{bmatrix} = (\boldsymbol{\Omega}_1)^{-1} \boldsymbol{\omega} = \frac{1}{2} \times \left[(\omega_1 + \omega_2)\mathbf{n} + (\omega_3 + \omega_4)\mathbf{n}_1 \times \times (\omega_2 - \omega_1)(\rho(c_p - c_3)\mathbf{N}_{00} + \rho c_3 \mathbf{I}) + 2\rho c_s (\omega_4 - \omega_3)\mathbf{N}_{01} + 2\omega_5 (\mathbf{I} - \mathbf{N}_{00})\right]. \tag{47}$$

In the three-dimensional case, the action of the matrix $(\boldsymbol{\Omega}_1)^{-1}$ from (20) on the vector $\boldsymbol{\omega}$ can be represented in the form

$$\begin{bmatrix} \mathbf{v} \\ \boldsymbol{\sigma} \end{bmatrix} = (\boldsymbol{\Omega}_1)^{-1} \boldsymbol{\omega} = \frac{1}{2}\left[(\omega_1 + \omega_2)\mathbf{n} + (\omega_3 + \omega_4)\mathbf{n}_1 + (\omega_5 + \omega_6)\mathbf{n}_2 \times \rho(\omega_2 - \omega_1)((c_p - c_3)\mathbf{N}_{00} + c_3 \mathbf{I}) \right. \\ \left. + 2c_s \rho(\omega_4 - \omega_3)\mathbf{N}_{01} + 2c_s \rho(\omega_6 - \omega_5)\mathbf{N}_{02} + 4\omega_7 \mathbf{N}_{12} + \omega_8(\mathbf{N}_{11} - \mathbf{N}_{22}) + \omega_9(\mathbf{I} - \mathbf{N}_{00})\right]. \tag{48}$$

In (47), (48), and in what follows, c_3 is defined as

$$c_3 = \frac{\lambda}{\lambda + 2\mu} c_p. \tag{49}$$

Consider a boundary corrector with a given external force density $\mathbf{f}$. In this case, conditions (22) and (23) become

$$\boldsymbol{\sigma} \cdot \mathbf{p} = \mathbf{f}. \tag{50}$$

Here and below, $\mathbf{p}$ denotes the outward normal vector to the boundary.

For a boundary corrector with a given boundary velocity $\mathbf{V}$, conditions (22), (23) become

$$\mathbf{v} = \mathbf{V}. \tag{51}$$

For a boundary corrector in mixed boundary conditions with a given normal boundary velocity V_p and a given tangential external force density $\mathbf{f}_\tau$, conditions (22) and (23) become

$$\mathbf{v} \cdot \mathbf{p} = V_p, \tag{52}$$

$$\boldsymbol{\sigma} \cdot \mathbf{p} = \mathbf{f}, \tag{53}$$

where

$$\mathbf{f} = \mathbf{f}_\tau + ((\mathbf{f} - \mathbf{f}_\tau) \cdot \mathbf{p})\mathbf{p}. \tag{54}$$

For the second boundary corrector in mixed boundary conditions with a given tangential boundary velocity $\mathbf{V}_\tau$ and a given normal external force density f_p, conditions (22) and (23) become

$$\mathbf{V} = \mathbf{V}_\tau, \tag{55}$$

$$\boldsymbol{\sigma} \cdot \mathbf{p} = \mathbf{f}, \tag{56}$$

$$\mathbf{f} \cdot \mathbf{p} = f_p. \tag{57}$$

Consider a nonreflecting boundary corrector. Then the differences between the values along characteristics (17) and (18) going beyond the integration domain must be zero, i.e.,

$$\mathbf{D} = \boldsymbol{\Omega}^{\text{out}}, \tag{58}$$

$$\mathbf{d} = 0, \tag{59}$$

where $\boldsymbol{\Omega}^{\text{out}}$ is the matrix composed of the columns of $\boldsymbol{\Omega}$ corresponding to the outgoing characteristics. Formulas (28) and (29) become

$$\boldsymbol{\Phi} = \boldsymbol{\Omega}^{*,\text{out}}(\boldsymbol{\Omega}^{\text{out}}\boldsymbol{\Omega}^{*,\text{out}})^{-1}, \tag{60}$$

$$\mathbf{F} = \mathbf{I} - \boldsymbol{\Omega}^{*,\text{out}}(\boldsymbol{\Omega}^{\text{out}}\boldsymbol{\Omega}^{*,\text{out}})^{-1}\boldsymbol{\Omega}^{\text{out}}. \tag{61}$$

In what follows, in the cases of contact correctors, we assume that a and b are bodies and $\mathbf{p}$ is the outward normal vector to the boundary of a.

For a contact corrector of the no-slip type, the conditions on the contact surface are specified as

$$\mathbf{v}^a = \mathbf{v}^b = \mathbf{V}, \tag{62}$$

$$\mathbf{f}^a = -\mathbf{f}^b. \tag{63}$$

For a contact corrector of the free slip type, the conditions set on the contact surface are

$$\mathbf{v}_a \cdot \mathbf{p} = \mathbf{v}_b \cdot \mathbf{p} = V_p, \tag{64}$$

$$f_p^a = -f_p^b, \tag{65}$$

$$f_\tau^a = f_\tau^b = 0. \tag{66}$$

ACOUSTIC MEDIA

To be definite, we consider the x direction. The action of the matrix $\mathbf{A}_1$ on the vector of unknowns defined as

$$\mathbf{q} = \begin{bmatrix} \mathbf{v} \\ p \end{bmatrix} = \begin{bmatrix} v_1 & v_2 & v_3 & p \end{bmatrix}^{\mathrm{T}} \tag{67}$$

in the three-dimensional case and as

$$\mathbf{q} = \begin{bmatrix} \mathbf{v} \\ p \end{bmatrix} = \begin{bmatrix} v_1 & v_2 & p \end{bmatrix}^{\mathrm{T}} \tag{68}$$

in the two-dimensional case can be written in the form

$$\mathbf{A}_1 \begin{bmatrix} \mathbf{v} \\ p \end{bmatrix} = \begin{bmatrix} \dfrac{p}{\rho}\mathbf{n} \\ c^2\rho(\mathbf{n}\cdot\mathbf{v}) \end{bmatrix}. \tag{69}$$

The matrices $\mathbf{A}_1^{3\mathrm{D}}$, $\mathbf{A}_2^{3\mathrm{D}}$, and $\mathbf{A}_3^{3\mathrm{D}}$ have the same set of eigenvalues:

$$\{c, -c, 0, 0\}. \tag{70}$$

The matrices $\mathbf{A}_1^{2\mathrm{D}}$ and $\mathbf{A}_2^{2\mathrm{D}}$also have the same ser of eigenvalues:

$$\{c, -c, 0\}. \tag{71}$$

In the two-dimensional case, the action of the matrix $\mathbf{\Omega}_1$ from (15) on the vector of unknowns (68) can be represented as

$$\omega_{1,2} = \left(\mathbf{\Omega}\begin{bmatrix} \mathbf{v} \\ p \end{bmatrix}\right)_{1,2} = \mathbf{n}\cdot\mathbf{v} \pm \frac{p}{c\rho}, \tag{72}$$

$$\omega_3 = \mathbf{n}_1\cdot\mathbf{v}. \tag{73}$$

In the three-dimensional case, the action of the matrix $\mathbf{\Omega}_1$ from (16) on the vector of unknowns (67) can be represented by (72), (73), and the expression

$$\omega_4 = \mathbf{n}_2\cdot\mathbf{v}. \tag{74}$$

In the two-dimensional case, the action of the matrix $(\mathbf{\Omega}_1)^{-1}$ from (19) on the vector $\boldsymbol{\omega}$ can be represented in the form

$$\begin{bmatrix} \mathbf{v} \\ p \end{bmatrix} = \mathbf{\Omega}^{-1}\boldsymbol{\omega} = \frac{1}{2}\begin{bmatrix} (\omega_1+\omega_2)\mathbf{n} + \omega_3\mathbf{n}_1 \\ c\rho(\omega_1-\omega_2) \end{bmatrix}. \tag{75}$$

In the three-dimensional case, the action of the matrix $(\mathbf{\Omega}_1)^{-1}$ from (20) on the vector $\boldsymbol{\omega}$ can be represented as

$$\begin{bmatrix} \mathbf{v} \\ p \end{bmatrix} = \mathbf{\Omega}^{-1}\boldsymbol{\omega} = \frac{1}{2}\begin{bmatrix} (\omega_1+\omega_2)\mathbf{n} + \omega_3\mathbf{n}_1 + \omega_4\mathbf{n}_2 \\ c\rho(\omega_1-\omega_2) \end{bmatrix}. \tag{76}$$

For a boundary condition with a given pressure, expressions (22) and (23) become

$$p^{n+1} = p. \tag{77}$$

The boundary corrector is given by the formulas

$$\mathbf{v}^{n+1} = \mathbf{v}^{\mathrm{in}} + \frac{p^{\mathrm{in}} - p}{c\rho}\mathbf{p}, \tag{78}$$

$$p^{n+1} = p. \tag{79}$$

For a boundary condition with a given normal velocity, (22) and (23) become

$$\mathbf{v}^{n+1}\cdot\mathbf{p} = V_p. \tag{80}$$

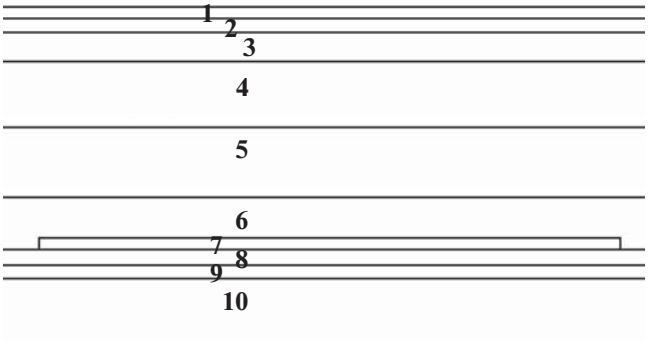

Fig. 1. Locations of ten layers in the problem.

The boundary corrector is given by the formulas

$$\mathbf{v}^{n+1} = \mathbf{v}^{\text{in}} - (\mathbf{v}^{\text{in}} \cdot \mathbf{p} - V_p)\mathbf{p}, \tag{81}$$

$$p^{n+1} = p^{\text{in}} + c_1\rho(\mathbf{v}^{\text{in}} \cdot \mathbf{p} - V_p). \tag{82}$$

Consider a contact corrector with conditions

$$\mathbf{v}_a \cdot \mathbf{p} = \mathbf{v}_b \cdot \mathbf{p} = V_p, \tag{83}$$

$$p^a = p^b. \tag{84}$$

Let p be given by the formula

$$p = \frac{c^a\rho^a p^{\text{in},b} + c^b\rho^b p^{\text{in},a} - c^a\rho^a c^b\rho^b((\mathbf{v}^{\text{in},b} \cdot \mathbf{p}) - (\mathbf{v}^{\text{in},a} \cdot \mathbf{p}))}{c^a\rho^a + c^b\rho^b}. \tag{85}$$

Substituting p into (78) and (79), we obtain the action of this contact corrector for both bodies.

COMPARISON OF WAVE PROCESSES IN LINEAR ELASTIC AND ACOUSTIC MEDIA

We considered a multilayered geological medium with layers schematically shown in Fig. 1. The integration domain was 12000 m wide, with the tenth layer being at a depth of 2601 m. The nonreflecting boundary conditions (58)–(61) were set on the lateral boundary of the integration domain. Condition (77)–(79) with a given pressure equal to zero was specified on the daytime surface. The source was placed at a depth of 6 m and was defined by a Ricker wavelet of frequency f:

$$f = \frac{\sqrt{6}}{\pi} f_{\text{M}}. \tag{86}$$

Here, f_{M} denotes a quantity equal to unity divided by the distance between the minima of the Ricker wavelet; it was equal to 40 Hz.

The receivers were also placed at a depth of 6 m and 4500 m away from the source on each side at intervals of 24 m. The time step was set to 0.00037 s, and 5001 time steps were taken. The grid in the 10th layer consisted of squares with a side length of 3 m, while a grid of 3 m by 2 m rectangles was used in the other layers.

Two formulations were used in the numerical simulation. In the first one, the first layer was filled with water. The parameters of all layers are given in Table. System (3), (4) was solved in the first layer, while system (1), (2), in the other layers. Conditions (31)–(33) were set at the interface between the first and second layers, while conditions (62) and (63) were specified on the other interfaces. In the second formulation, system (3), (4) was solved in all layers, the velocity c was specified as that of longitudinal P-waves in the corresponding layer, and conditions (83)–(85) were set at all interfaces. In both formulations, the seventh layer was a hydrocarbon reservoir.

Figures 2–7 present the wave patterns at the times $t = 0.4514$, 0.6438, 0.6808, 0.8991, 1.332, and 1.85 s, respectively. The magnitude of the velocity is shown in shades of gray. In Fig. 2–6, the left side of the integration domain for the second formulation is presented on the left, while the right side of the integration

Seismic characteristics of ten layers

Layer index	Density, kg/m^3	Speed of P-waves, m/s	Speed of S-waves, m/s	Layer thickness, m
1	1000	1500	–	60
2	2300	3200	1960	70
3	2300	3700	2260	150
4	2400	4000	2450	340
5	2500	4300	2630	360
6	2600	4500	2750	270
7	2300	3200	1700	60
8	2600	4600	2820	80
9	2700	4800	2940	70
10	2800	5400	3300	2601

domain for the first formulation is shown on the right; in different figures, the regions have different sizes. Figure 7 displays an upper part of the integration domain for the second formulation (upper half of the figure) and for the first formulation (lower half). The receivers were also placed at a depth of 6 m and 4500 m away from the source on each side at intervals of 24 m. Figure 8 shows the seismograms [26] produced by the receivers to the left of the source for the second formulation (left half) and to the right of the source for the first formulation (right half). For illustrative purposes, multiple waves were eliminated from the water layer in the computations.

In Figs. 2 and 7, P-waves from the source are labeled by P; Stoneley waves in water, by St; and the S-waves induced by the P-waves, by S. In Fig. 2, PP-waves reflected from the top of the reservoir are labeled by PP1; PP-waves reflected from the bottom of the reservoir, by PP2; the exchange PS-wave reflected from the top of the reservoir, by PS1; and the exchange PS-wave reflected from the bottom of the reservoir, by PS2. In Fig. 3, SP1 marks the exchange SP-wave reflected from top of the reservoir; SP2 marks the exchange SP-wave reflected from bottom of the reservoir; SS1 and SS2 mark SS-waves reflected from the top and bottom of the reservoir, respectively; and rPP1 labels the responses to PP1-waves in the water layer. The letters rPP2 in Fig. 4 denote the responses to PP2-waves in the water layer. In Fig. 5, rPS1 and rPS2 label the responses to PS1- and PS2-waves in the water layer. In Fig. 6, rSS1 and rSS2 denote the responses to SS1- and SS2-waves in the water layer.

It can be seen that the numerical results obtained by solving the acoustic field system (3), (4) do not contain Stoneley waves (St), S-waves (S), exchange PS-waves reflected from the reservoir top and bottom (PS1, PS2), SS-waves reflected from the reservoir top and bottom (SS1, SS2), exchange SP-waves

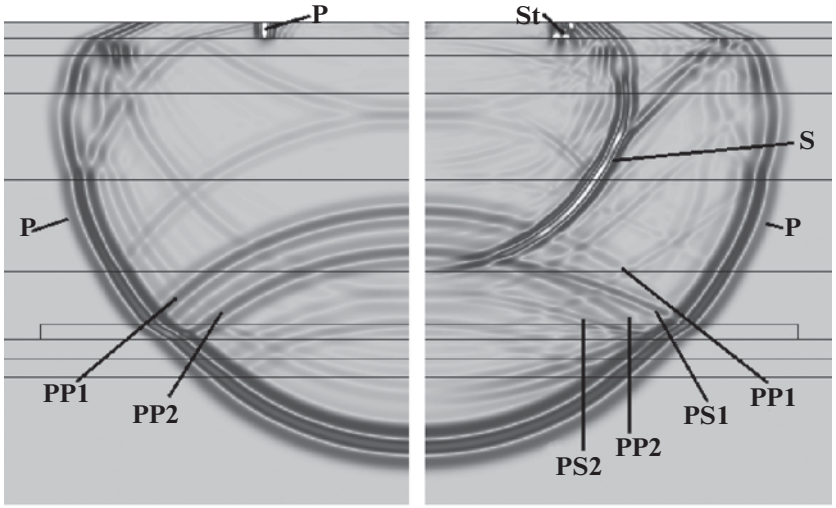

Fig. 2. Wave patterns at $t = 0.4514$ s. Reflection of a P-wave from the reservoir.

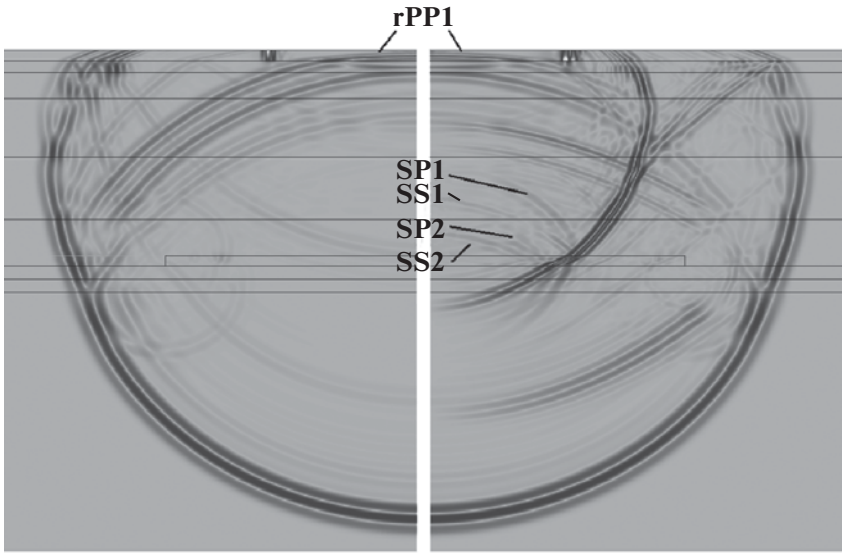

Fig. 3. Wave patterns at $t = 0.6438$ s. Reflection of an S-wave from the reservoir.

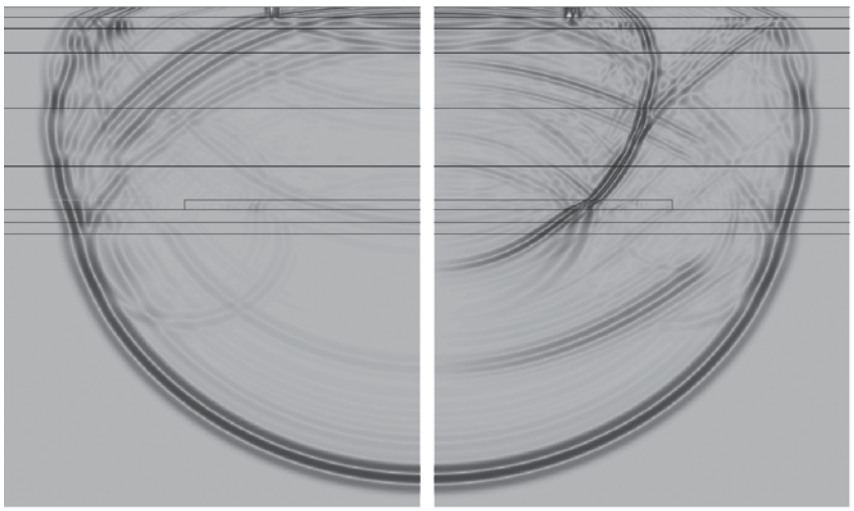

Fig. 4. Wave patterns at $t = 0.6808$ s. Water response to the reservoir.

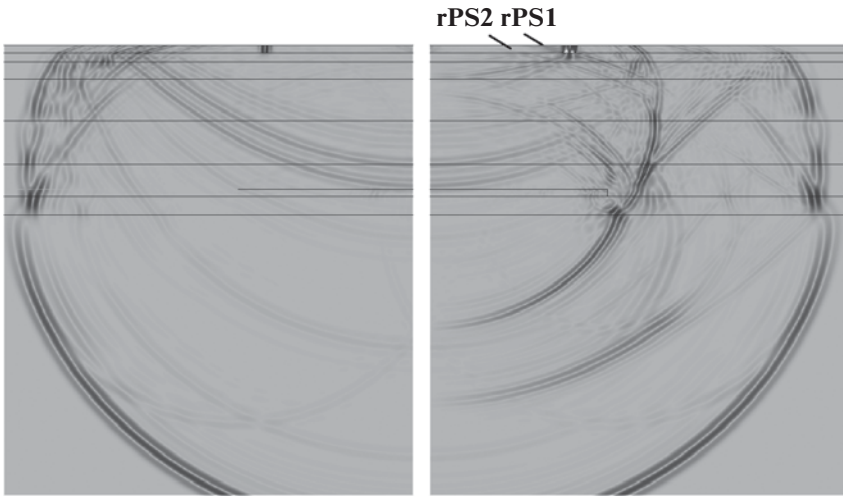

Fig. 5. Wave patterns at $t = 0.8991$ s. Water response to the reservoir.

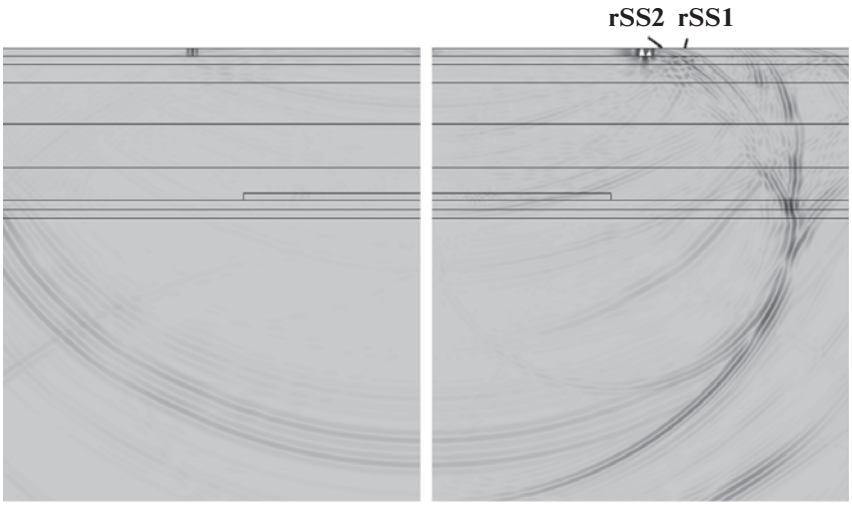

Fig. 6. Wave patterns at $t = 1.332$ s. Water response to the reservoir.

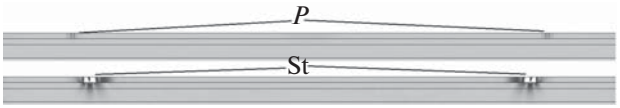

Fig. 7. Wave patterns at $t = 1.85$ s. Stoneley waves.

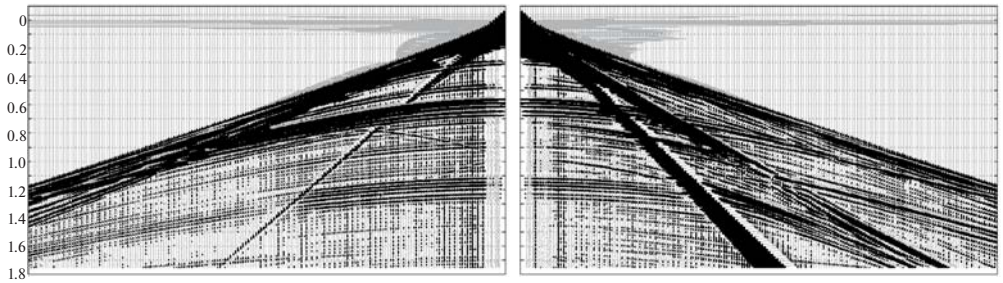

Fig. 8. Seismograms.

reflected from the reservoir top and bottom (SP1, SP2) and, accordingly, the responses to them in the water layer (rPS1, rPS2, rSS1, rSS2, rSP1, rSP2). These differences are also manifested in the seismograms showing the vertical velocity (Fig. 8).

WAVE PROPAGATION IN THE PRESENCE OF ICEBERGS

The integration domain was a parallelepiped 120 m long, 120 m wide, and 60 m deep. The simulated medium was defined as a multilayer system consisting of a water layer with two icebergs and a bottom rock layer with a hydrocarbon sublayer.

The computations were performed on a rectangular grid with 5.4×10^7 nodes. The initial point perturbation was specified by a Ricker wavelet of frequency 42.85 Hz. The nonreflecting boundary conditions (58)–(61) were set on the lateral boundaries of the integration domain. There were 15000 time steps taken in the run. A single time step was 3×10^{-5} s. The spatial step was equal to 0.4 m. The icebergs were 12 m × 64 m × 12 m and 12 m × 12 m × 12 m in size with their bottom surfaces at a depth of 12 meters and with their top surfaces being 1 m above the water. The ice density was set to 917 kg/m^3, and the speeds of P- and S-waves waves in the ice were specified as 394 and 2491 m/s, respectively. On the visible surfaces of the

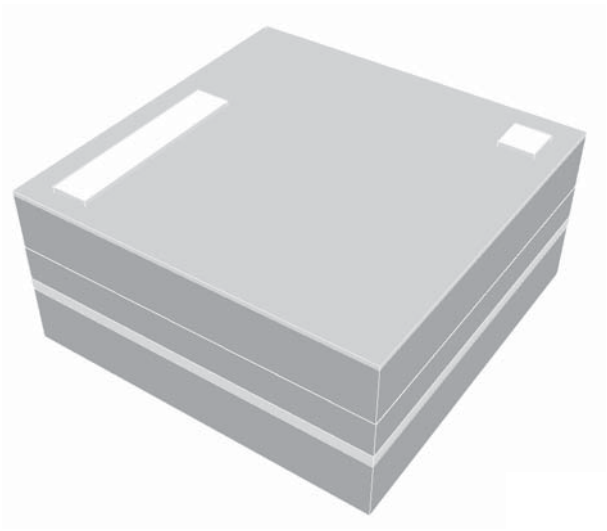

Fig. 9. Formulation of the problem.

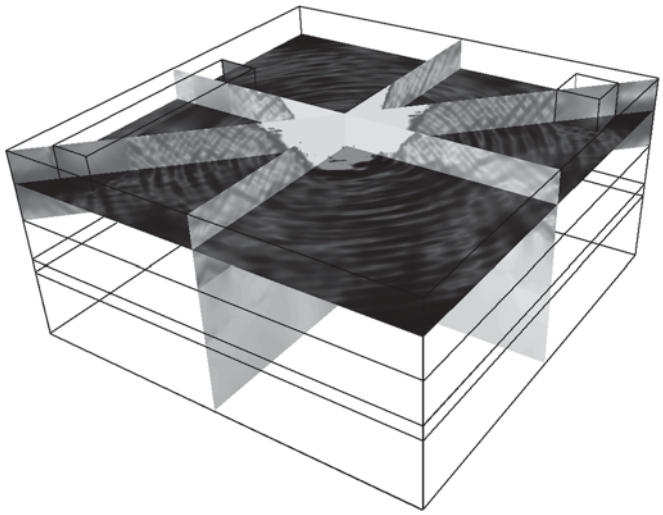

Fig. 10. Water waves reflected from the icebergs.

icebergs, we used condition (50) with the external force density set equal to zero. On the upper water surface, we specified conditions (77)–(79) with the pressure set equal to zero. The water layer was 20 m thick with a density of 1000 kg/m^3 and speed of sound 1500 m/s. For a rock density of 2500 kg/m^3, the speeds of P- and S-waves were set to 6500 and 3700 m/s, respectively. The density of the hydrocarbon inclusion was specified as 2000 kg/m^3 with respective wave speeds of 4000 and 1250 m/s. The formulation of the problem is shown in Fig. 9. Figure 10 presents the wave pattern at $t = 0.195$ s.

CONCLUSIONS

For the task of seismic exploration on the Arctic shelf, we compared wave processes and seismograms numerically computed in the case of rock modeled as a linear elastic medium and an acoustic medium. It was found that, in contrast to the linear elasticity system, the acoustic field system fails to reproduce

—Stoneley waves;

—S-waves in rock induced by P-waves propagating from a source located near the water surface;

—exchange PS-waves reflected from the top and bottom boundaries of the reservoir;

—SS-waves reflected from the top and bottom boundaries of the reservoir;

—exchange SP-waves reflected from the top and bottom boundaries of the reservoir;

—water responses to the above waves reflected from the reservoir.

These differences are also manifested in the seismograms showing the vertical velocity.

Additionally, the influence of ice structures (icebergs) on wave processes arising in seismic exploration on the Arctic shelf was investigated. The numerical simulation was based on the grid-characteristic method, which correctly describes wave processes in the problems under study and does not fail near the boundaries and interfaces of the integration domain. The linear elasticity system and the acoustic field system were jointly solved in this work.

ACKNOWLEDGMENTS

This work was supported by the Ministry of Education and Science of the Russian Federation, contract no. 14.575.21.0084 of October 20, 2014 (applied research identifier RFMEFI57514X0084).

REFERENCES

1. W. Goodway and M. Enachescu, "Introduction to this special section: Arctic/ATC," The Leading Edge **32** (5), 522–523 (2013).
2. A. B. Baggeroer and G. L. Duckworth, "Seismic exploration in the Arctic Ocean," The Leading Edge **2** (10), 22–27 (1983).
3. D. C. Henley, "Attenuating the ice flexural wave on arctic seismic data," *SEG Technical Program Expanded Abstracts* (2006), pp. 2757–2761.
4. R. Trupp, J. Hastings, S. Cheadle, and R. Vesely, "Seismic in arctic environs: Meeting the challenge," The Leading Edge **28** (8), 936–942 (2009).
5. D. C. Mosher, C. B. Chapman, J. Shimeld, H. R. Jackson, D. Chian, J. Verhoef, D. Hutchinson, N. Lebedeva-Ivanova, and R. Pederson, "High arctic marine geophysical data acquisition," The Leading Edge **32** (5), 524–536 (2013).
6. S. L. Rice, T. Dudley, C. Schneider, R. J. Pierce, B. Horn, S. Cameron, R. Bloor, and Z.-Z. J. Zhou, "Arctic seismic acquisition and processing," The Leading Edge **32** (5), 546–554 (2013).
7. B. R. Julian and D. Gubbins, "Three-dimensional seismic ray tracing," J. Geophys. **43**, 95–113 (1977).
8. A. Bermudez, L. Hervella-Nieto, and R. Rodriguez, "Finite element computation of three-dimensional elasto-acoustic vibrations," J. Sound Vibration **219** (2), 279–306 (1999).
9. M. Kazer and M. Dumbser, "A highly accurate method for complex interfaces between solids and moving fluids," Geophysics **73** (3), 723–725 (2008).
10. R. Van Vossen, J. O. A. Robertsson, and C. H. Chapman, "Finite-difference modeling of wave propagation in a fluid-solid configuration," Geophysics **67** (2), 618–624 (2002).
11. J. De la Puente, M. Kaser, M. Dumbser, and H. Igel, "An arbitrary high-order discontinuous Galerkin method for elastic waves on unstructured meshes IV: Anisotropy," Geophys. J. Int. **169**, 1210–1228 (2007).
12. G. Seriani, E. Priolo, J. M. Carcione, and E. Padovani, "High-order spectral element method for elastic wave modeling," *Extended Abstracts of the 62nd Annual International Meeting and Exposition* (SEG, 1992), pp. 1285–1288.
13. A. Levander, "Fourth-order finite-difference P-SV seismograms," Geophysics **53** (11), 1425–1436 (1988).
14. S. Vlastos, E. Liu, I. G. Main, and X.-Y. Li, "Numerical simulation of wave propagation in media with discrete distributions of fractures: Effect of fracture size and spatial distributions," Geophys. J. Int. **152** (3), 649–668 (2003).
15. A. V. Favorskaya, I. B. Petrov, A. V. Sannikov, and I. E. Kvasov, "Grid-characteristic method using high order interpolation on tetrahedral hierarchical meshes with a multiple time step," Math. Models Comput. Simul. **5** (5), 409–415 (2013).
16. A. V. Favorskaya, D. I. Petrov, I. B. Petrov, and N. I. Khokhlov, "Numerical solution of arctic problems by applying the grid-characteristic method," Izv. Yuzh. Fed. Univ. Tekh. Nauki, No. **12**, 192–200 (2014).
17. V. I. Golubev, I. B. Petrov, and N. I. Khokhlov, "Numerical simulation of seismic activity by the grid-characteristic method," Comput. Math. Math. Phys. **53** (10), 1523–1533 (2013).

18. K. M. Magomedov and A. S. Kholodov, *Grid-Characteristic Numerical Methods* (Nauka, Moscow, 1988) [in Russian].
19. I. B. Petrov and A. S. Kholodov, "Numerical study of some dynamic problems of the mechanics of a deformable rigid body by the mesh-characteristic method," USSR Comput. Math. Math. Phys. **24** (3), 61–73 (1984).
20. I. B. Petrov and A. S. Kholodov, "Regularization of discontinuous numerical solutions of equations of hyperbolic type," USSR Comput. Math. Math. Phys. **24** (4), 128–138 (1984).
21. I. B. Petrov, A. G. Tormasov, and A. S. Kholodov, "On the use of hybrid grid-characteristic schemes for the numerical solution of three-dimensional problems in the dynamics of a deformable solid," USSR Comput. Math. Math. Phys. **30** (4), 191–196 (1990).
22. I. E. Kvasov and I. B. Petrov, "High-Performance computer simulation of wave processes in geological media in seismic exploration," Comput. Math. Math. Phys. **52** (2), 302–313 (2012).
23. W. Nowacki, *Teoria Sprezystosci* (Panstwowe Wydawnictwo Naukowe, Warsaw, 1970; Mir, Moscow, 1975).
24. L. D. Landau and E. M. Lifshitz, *Theory of Elasticity* (Butterworth-Heinemann, Oxford, 1986; Nauka, Moscow, 1987).
25. A. V. Favorskaya, I. B. Petrov, and K. A. Beklemysheva, "Numerical simulation of processes in solid deformable media in the presence of dynamic contacts using the grid-characteristic method," Math. Models Comput. Simul. **6** (3), 294–304 (2014).
26. V. I. Golubev, "Method for visualizing and interpreting results of full-wave seismic computations," Tr. Mosk. Fiz.-Tekh. Inst. **6** (1), 154–161 (2014).

Translated by I. Ruzanova

SPELL: OK